



**HAL**  
open science

## Salt leaching using powder (SLUP) process for glass/chitosan scaffold elaboration for biomaterial applications

Jibed Refifi, Hassane Oudadesse, O. Merdrignac-Conanec, Hafed El Feki, Bertrand Lefeuvre

### ► To cite this version:

Jibed Refifi, Hassane Oudadesse, O. Merdrignac-Conanec, Hafed El Feki, Bertrand Lefeuvre. Salt leaching using powder (SLUP) process for glass/chitosan scaffold elaboration for biomaterial applications. *Journal of The Australian Ceramic Society*, 2020, 56 (3), pp.1167-1178. 10.1007/s41779-020-00460-6 . hal-02797031

**HAL Id: hal-02797031**

**<https://univ-rennes.hal.science/hal-02797031>**

Submitted on 17 Jun 2020

**HAL** is a multi-disciplinary open access archive for the deposit and dissemination of scientific research documents, whether they are published or not. The documents may come from teaching and research institutions in France or abroad, or from public or private research centers.

L'archive ouverte pluridisciplinaire **HAL**, est destinée au dépôt et à la diffusion de documents scientifiques de niveau recherche, publiés ou non, émanant des établissements d'enseignement et de recherche français ou étrangers, des laboratoires publics ou privés.

# Salt leaching using powder (SLUP) process for glass/chitosan scaffold elaboration for biomaterial applications

Jihen Refifi<sup>1,2</sup> · Hassane Oudadesse<sup>1</sup> · O. Merdrignac-Conanec<sup>1</sup> · Hafed El Feki<sup>2</sup> · Bertrand Lefevre<sup>1</sup>

<sup>1</sup> CNRS, ISCR-UMR 6226, University Rennes, F-35000 Rennes, France

<sup>2</sup> Laboratory of Materials Sciences and Environment, University of Sfax, 3038 Sfax, Tunisia

## Abstract

Tissue engineering has emerged as an alternative approach to create bone tissue by growing cells on 3D scaffolding. The aim of this study was to synthesize a composite glass/chitosan (BG-CH) by using new salt leaching using powder (SLUP) process in order to control the porosity rate and then the chemical reactivity of the final product. SLUP process consists on the cavity creation with desired pore sizes. It does not require heat treatment. This process is based on washing out the NaCl particles used for that. It is due to its high solubility in aqueous media. This work focuses on the elaboration, physicochemical, and chemical reactivity studies of pure bioactive glass and bioactive glass associated with chitosan. A range of composite scaffolds with different bioactive glass/chitosan contents has been synthesized. NaCl with a distinct range size was used with the aim of optimizing the pore network. Obtained results show that the specific surface area and pore volume increase with increasing of chitosan and porogen content. The same observations for pore volume were registered. The obtained scaffolds had high porosity (90%) with good pore connectivity. SEM images revealed strong dependence of sizes and shapes of pores on the salt/composite ratios.

**Keywords** Bioactive glass · Chitosan · Biomaterial · Salt leaching using powder · Porosity

## Introduction

Large, nonhealing bone defects caused by trauma, tumor resection, or disease pose major clinical and socioeconomic problems. In situations with significant bone loss, bone grafts are used to fill the defect bone and promote bone tissue formation [1, 2]. More than 500,000 bone-grafting procedures are performed every year [3]. This number is projected to increase steadily due to population aging and correspondingly rising incidence of degenerative musculoskeletal diseases. At present, there is no ideal treatment for large bone defects. Bone allografts could be interesting; however, their clinical utility is limited by the risk of disease transmission and high cost [4–6]. To overcome the shortcomings of bone grafting, much research effort is focused on the development of

synthetic bone scaffolds as bone graft substitutes. They are widely regarded to be one of the key items along with cells and a dynamic environment for regeneration of damaged tissue [7–9]. Scaffolds are three-dimensional porous structures that act as templates for in situ bone regeneration. The successful design of a bone scaffold needs to incorporate both biological physicochemical and mechanical considerations [10]. The basic biological requirement of any bone scaffold is osteoconductivity, i.e. the ability to support the attachment of bone cells and to provide an interconnected pore structure through which cell migration and vessel formation can take place. To satisfy these conditions, scaffolds need well-interconnected pores and suitable porosity [11, 12] and large specific surface and uniform pore distribution with a degradation or resorption rate that the tissue replacement needs [13]; also, it needs to be biocompatible and biodegradable. Scaffolds are desired to minimize the amount of implanted material and to increase the specific surface area for cell attachment, a vibrant environment for regeneration of damaged tissue and tissue in growth [14, 15]. Cells are developed on a biodegradable porous scaffold in which the tissue is forming and growing; the scaffold gradually degrades.

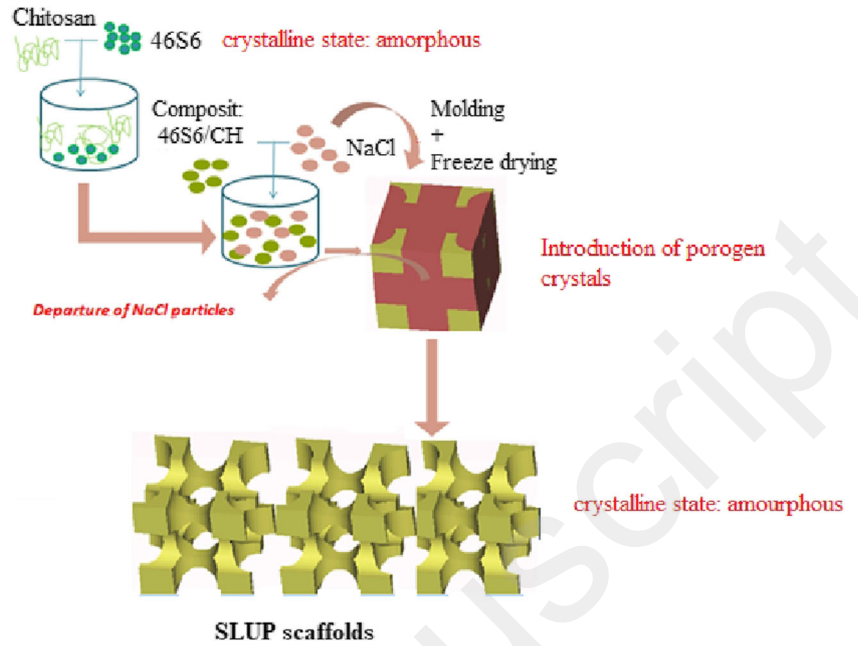
For this reason, several methods have been developed to prepare porous scaffolds with well pore interconnectedness



hassane.oudadesse@univ-rennes1.fr



Fig. 1 SLUP process



159 According to the technique and chitosan rate, they were sim- 179  
 160 ply called SLUPS29, SLUPS50, SLUPS71, and SLUPS90. 180

161 **Preparation of lyophilized scaffolds LS**

162 The same range was synthesized by using lyophilization pro- 180  
 163 cess: The first step has consisted to dissolve chitosan powder, 181  
 164 with a medium molecular weight, in acetic acid solution 1% 182  
 165 v/v. The solution was stirred under magnetic stirring at room 183  
 166 temperature during 24 h in order to dissolve all the chitosan 184  
 167 powder. The final step is the preparation of four scaffolds 185  
 168 having the same CH and BG ratio as those prepared by 186  
 169 SLUP method: LS:29CH, LS:50CH, LS:71CH, and 187  
 170 LS:90CH presenting different ratios chitosan/glass (CH/BG). 188  
 171 The glass was added in the chitosan solution. The mixtures 189  
 172 were homogenized for 24 h in an ultrasonic bath. The solu- 190  
 173 tions were cast into well plates. They were frozen at -20 °C 191  
 174 all-night to freeze the core of the material and placed in a 192  
 175 freeze-dryer at 0.65 mbar at -60 °C during 24 h to remove 193  
 176 all solvents in samples. Obtained scaffolds were washed in a 194  
 177 NaOH solution 0.4% w/v and distilled water to eliminate 195  
 178 traces of acetic acid. 196

179 **Physicochemical characterization of scaffolds**

180 To verify that the synthesized material is an amorphous glass, 180  
 181 its structure has been studied by using X-ray diffraction 181  
 182 (XRD). XRD measurements were performed with a PAN ana- 182  
 183 lytical model operate at 40 kV and 30 mA using Cu K $\alpha$  183  
 184 radiation. The detector was scanned over a range of 2 $\theta$  angles 184  
 185 from 5° to 90° at a step size of 0.026° and well time of 40 s per 185  
 186 step. The Fourier transform infrared spectroscopic analysis 186  
 187 (FT-IR) was used to determine the functional groups com- 187  
 188 posed the obtained scaffolds. A Bruker Equinox 55 spectrom- 188  
 189 eter was employed for the FT-IR spectroscopy analysis. The 189  
 190 samples of scaffolds powders were mixed with KBr powder 190  
 191 and pressed into a disk suitable for FT-IR measurement. The 191  
 192 FT-IR spectra were recorded from 4000 to 400 cm<sup>-1</sup>. The 192  
 193 morphology of the scaffolds was observed using scanning 193  
 194 electron microscopy (SEM) (Jeol JSM 6301). The flow of 194  
 195 electrical charges at the surface is necessary for the SEM anal- 195  
 196 ysis. For that, samples have been metalized by gold-palladium 196  
 197 layer (a few  $\mu$ m of thickness). 197

198 Specific surface area and pore size distribution of the sam- 198  
 199 ples have been calculated by using Brunauer–Emmett–Teller 199

t1.1 **Table 1** Chemical composition of scaffolds

t1.2 Sample	Solvent volume 1% (ml)	Mass of chitosan (g)	Concentration of the chitosan solution (%)	Mass of used glass (g)	% by weight of chitosan in composites	Composite notation	NaCl/Composite
t1.3 SLUP29	80	0.80	1	2.00	29	46S6:29CH	1
t1.4 SLUP50	140	1.40	1	1.40	50	46S6:50CH	1
t1.5 SLUP71	200	2.00	1	0.80	71	46S6:71CH	1
t1.6 SLUP90	252	2.52	1	0.28	90	46S6:90CH	1

200 (BET) N<sub>2</sub> adsorption-desorption method (Flowsorb II 2300,  
201 Coultronics France SA).

202 The Helium Pycnometer device measured porosity of the  
203 scaffolds. The experiments were performed five times, and the  
204 average porosity value was obtained. The porosity (P) of the  
205 scaffolds was obtained by the following equation.  
206

$$\text{Porosity} = \frac{V_0 - \frac{m}{\rho}}{V_0} \times 100(\%)$$

208 where

209 V<sub>0</sub>: The apparent volume of scaffold, which is calculated  
210 using the outer dimension of scaffold;

211 m: Mass of scaffold from which NaCl is leached out;

212 ρ: Density of sample. The following curve shows the evolu-  
213 tion of porosity rate according to the composition of SLUP  
214 scaffolds from 73 to 90%.

## 215 In vitro chemical reactivity study

216 In vitro assays, as described in a previous work [31], were  
217 realized in a SBF whose the chemical composition is similar  
218 to the blood plasma (Table 2) [31, 32]. A total of 30 mg of  
219 powder samples were immersed in triplicate in 60 ml of SBF  
220 at a temperature of 37 °C and maintained under controlled  
221 stirring at 50 rpm. At the end of soaking time, the powder  
222 samples were removed and rinsed with deionized water to  
223 stop the exchange reactions. The powder samples were dried  
224 and stored for further investigation of the formation of HA  
225 layer on the surface of powder samples. This hypothesis was  
226 verified by X-ray diffraction. The SBF solutions were stored  
227 in fridge to evaluate the ionic exchanges between materials  
228 and SBF by ICP-OES (Spectro Ciros Vision Ametek).

## 229 Results and discussion

### 230 Morphological study of scaffolds

#### 231 Binocular microscopy

232 The obtained images of SLUP scaffolds before and after the  
233 salt leaching using binocular microscopy are shown in Fig. 2.

t2.1 **Table 2** Ion concentrations (mM) in SBF and in human blood plasma [32]

t2.2		Na <sup>+</sup>	K <sup>+</sup>	Ca <sup>2+</sup>	Mg <sup>2+</sup>	Cl <sup>-</sup>	HCO <sub>3</sub> <sup>-</sup>	HPO <sub>4</sub> <sup>2-</sup>
t2.3	SBF	142	5	2.5	1.5	148.8	4.2	1
t2.4	Blood plasma	142	5	2.5	1.5	103	27	1

234 The porogen was used with the aim of optimizing the pores  
235 network; the solid porogen agent spreads in the structure in a  
236 controlled manner. It makes it possible to have better control  
237 of the pore size, particularly access to large sizes and better  
238 control of the pore's organization. The porogenic agent chosen  
239 (in particulate form, preferably (quasi-spherical) may be pref-  
240 erentially removed to obtain the porous layer whose pores  
241 may have substantially the shape and size of this pore-  
242 forming agent.

243 As depicted in Fig. 2, porosity appears in Fig. 2a just after  
244 salt-leaching out. The obtained images show that the compos-  
245 ite before leaching (Fig. 2a) is characterized by a compact  
246 surface covered by a layer of porogen. After leaching (Fig.  
247 2b), we clearly observe a radical change in the surface of the  
248 composite with the appearance of an organized porosity that  
249 occupies the entire surface of the composite. The efficiency of  
250 the process is directly related to the porogen.

#### 251 SEM

252 Morphology of the surface and of the interconnectivity of the  
253 fabricated scaffolds is presented in Fig. 3. Porous structure  
254 was observed on both; lyophilized scaffolds (Fig. 3a) and  
255 SLUP scaffold (Fig. 3b) at BG:chitosan contents of 50:50. A  
256 regular porous structure was observed in SLUPS; however,  
257 that of LS was irregular.

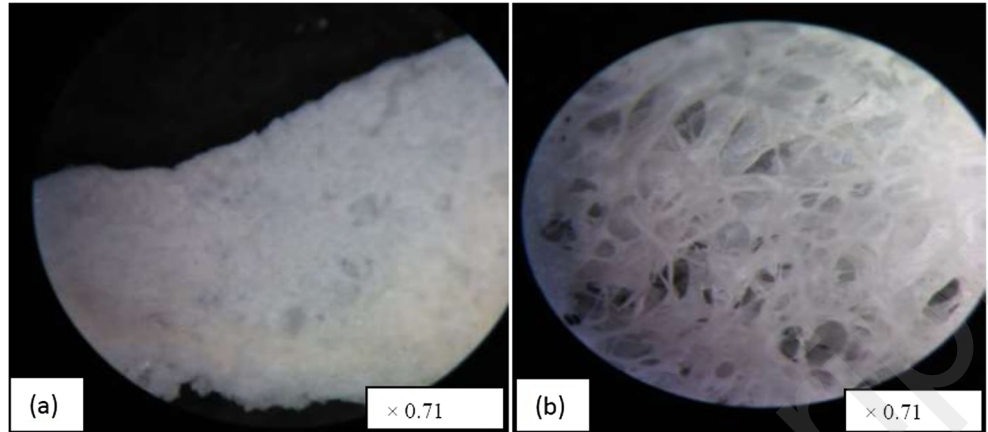
258 From a morphological point of view, the porosity of SLUP  
259 scaffold is much greater than that of LS scaffolds. SEM im-  
260 ages showed the influence of the salt particles on the pore size.  
261 It highlights the form and pore size uniformity. It shows the  
262 surface image and macrostructure of original salt-leaching  
263 scaffold with NaCl treatment. It demonstrates that pores create  
264 an interconnected network and are ideal for the vasculariza-  
265 tion. Therefore, the microstructure of the SLUP scaffolds is  
266 extremely promising since it is highly porous, with a well-  
267 developed network of interconnected pores.

268 This analysis aims also to observe the distribution and archi-  
269 tecture of the pores and to understand the association be-  
270 tween bioactive glass and chitosan matrix in a regular poros-  
271 ity. We have noticed from the SEM images that this phenom-  
272 enon is very important in the SLUP scaffolds. Good intercon-  
273 nectivity of the global pores was observed, and the coexist-  
274 ence of orders in obtained pores was verified.

275 The pores and caves structure in each sample can be clearly  
276 observed; with the pore size of around 30 μm sieving process  
277 in the SLUP scaffold (Fig. 3a) and heterogeneous pore size in  
278 the lyophilized scaffold as depicted in Fig. 3b.

279 Image of lyophilized scaffold (Fig. 3b) showed irregular  
280 pore structure and hole presence. There are no distinct and  
281 deep pores. The size and the shape of the pores were nonuni-  
282 form, and the pores tended to be piled up pell-mell with each  
283 other. For tissue engineering applications, irregular structure is  
284 unfavorable for the cell migration and growth because of the

**Fig. 2** Images of SLUP scaffolds before (a) and after (b) the salt leaching using binocular microscopy



285 pore architecture wish going from the surface to interior of  
 286 matter. However, the pore structure became more and more  
 287 clear and integral with the increase of NaCl content.  
 288 Especially, obvious honeycomb-like structure could be ob-  
 289 served especially in the samples with higher NaCl (NaCl:  
 290 composite = 1) as shown in Fig. 3a. Upon salt particles, the  
 291 obtained results show a soft structure with regular pores.  
 292 Before leaching, there is a lot of obvious configuration like  
 293 oval-shaped salt powder, which is leached out. The  
 294 picnometric measurements revealed that 90% of pore size  
 295 corresponds to the particle size of NaCl used as porogen.

The salt particles spread to the bottom of the scaffold ma-  
 trix creating a high porosity as shown in Fig. 4. Therefore, the  
 porosity of SLUP scaffold is higher than that of traditional  
 scaffold. The porosity of the material is one of the key param-  
 eters successes in tissue engineering applications. Its pore vol-  
 ume (void volume inside), pore size, and specially the inter-  
 connection between pores have a major influence on the abil-  
 ity of the bone-implant vascularization and gradually biomin-  
 eralization. They subsequently influence adhesion, cell migra-  
 tion, and tissue penetration within structures. It is therefore an  
 important parameter for tissue engineering. Other studies have

**Fig. 3** Morphology of the surface and of the interconnectivity of the fabricated scaffolds. **a** Lyophilized scaffolds; **b** SLUP scaffold

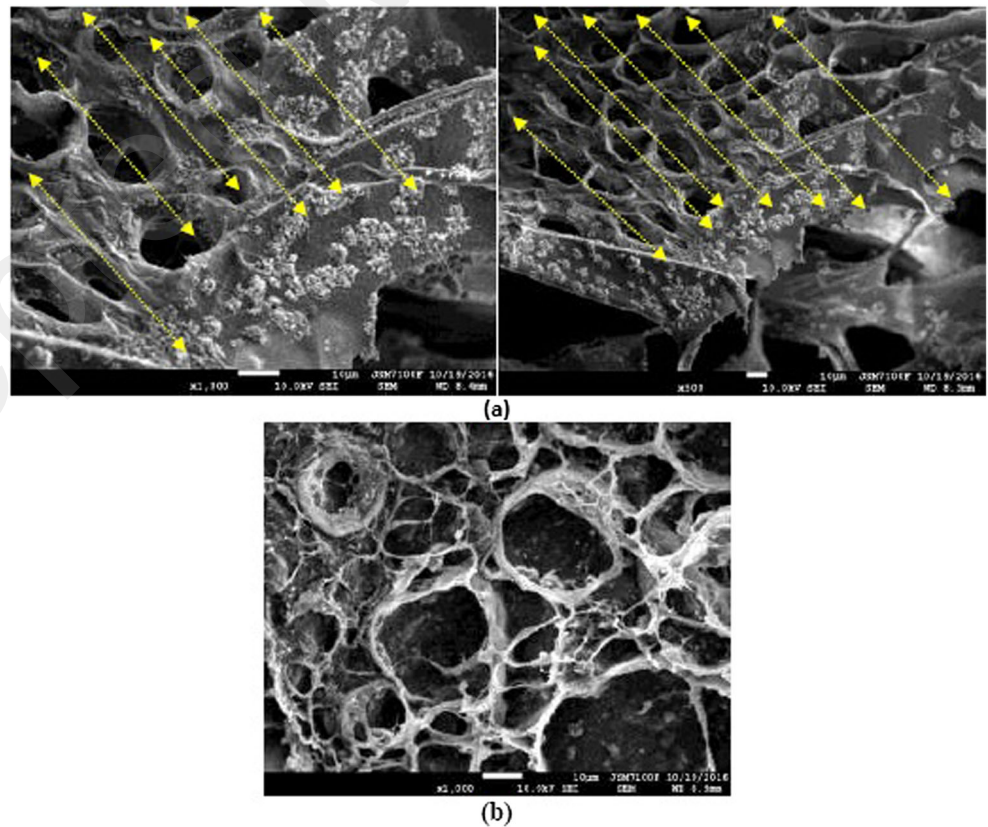
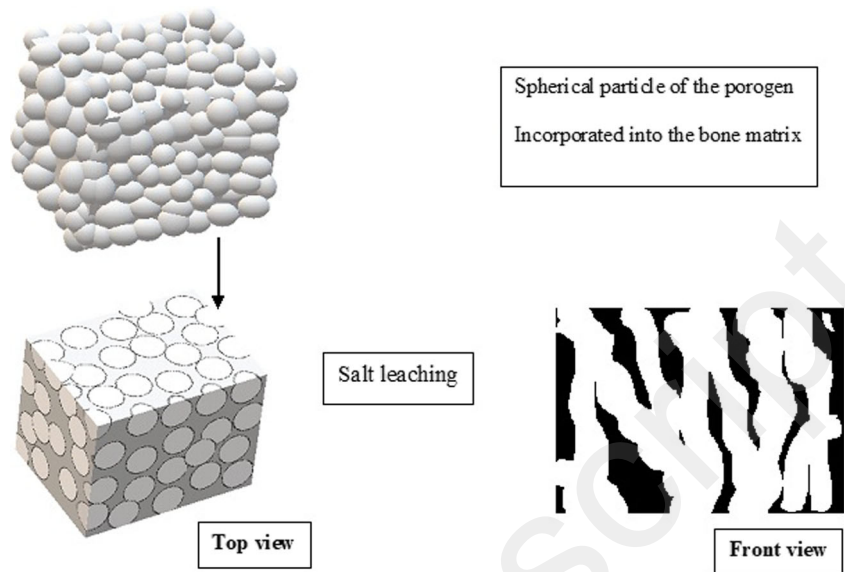


**Fig. 4** Salt particles spread to the bottom of the scaffold matrix creating a high porosity



307 reported that the induced porogen on the composite matrix  
308 generates a regular porosity [27, 33].

### 309 XRD and BET

310 The obtained diffractograms are presented in Fig. 5. The  
311 46S6-CH composite before the addition of porogen presents a  
312 diffraction halo between 16 and 24 ( $2\theta^\circ$ ) that we also observe  
313 on the diffractogram of chitosan alone. We also note the appearance  
314 of a halo at 30 ( $2\theta^\circ$ ) which highlights interactions  
315 between bioactive and chitosan. After the addition of porogen,  
316 we notice the appearance of the peaks corresponding to NaCl  
317 (31.8 and 45.4 ( $2\theta^\circ$ )), which disappear just after salt-leaching  
318 out. They assert that the crystalline structure of the scaffolds

after salt leaching retains its amorphous starting structure,  
which proves that the totality of porogen was leached out even  
that incorporated on the scaffolds structure leaving voids inter-  
connected between them. After water leaching, the NaCl  
was dissolved in water and the peaks of this phase in the  
XRD pattern disappeared accordingly after salt-leaching out  
as shown in Fig. 1, and no streak attributed to NaCl was  
detected on the scaffold diffractogram. This result was also  
confirmed by EDS analysis as shown in Fig. 6, which shows  
the disappearance of the porogen within the matrix of the  
composite.

### Porosity calculation

SLUP scaffolds possessed highest porosity (90%) as present-  
ed in Fig. 7. The high porosity of a scaffold can provide ben-  
efits for cell growth and migration. We observe more that the  
BG/CH ratio decreases towards a more porous structure.  
Table 3 presents the evolution of porosity rate according to  
the composition of our SLUP scaffolds and LS. Open porosity  
varies from 73 to 90% of SLUP when the open porosity rate of  
LS was too low and varies from 12 to 31%.

Comparing SLUPS with LS, BET measures show an im-  
portant evolution of pore volume in the case of SLUPS instead  
of LS as depicted in Fig. 8. In the case of LS, the pore volume  
varies between 3.8 and 6.5  $\text{mm}^3 \text{g}^{-1}$  depending on the BG:CH  
ratio. However, it varies between 5 and 6 in the case of SLUP  
scaffolds.

This characteristic justifies more and more the advantages  
of the technique “SLUP” and allows us to understand the  
physical behavior at the interior of the scaffolds matrix. In  
fact, SLUP is pressure free; there was a definite space between  
the powder particles, and this space does not shrink while  
melting composite, which leads to create a large pore volume.

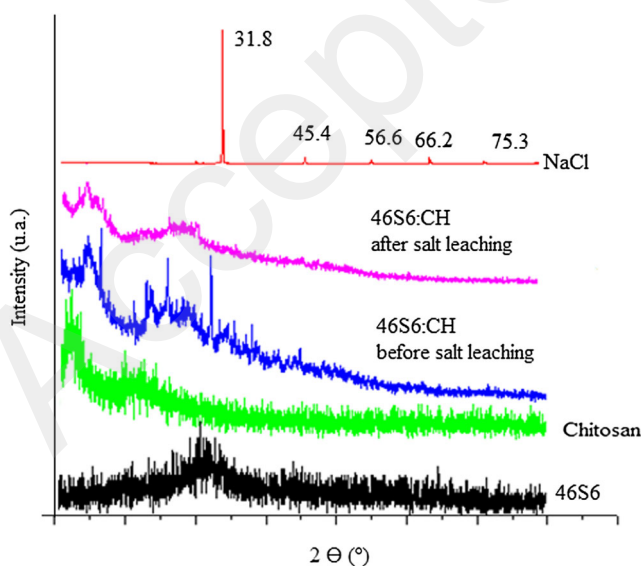
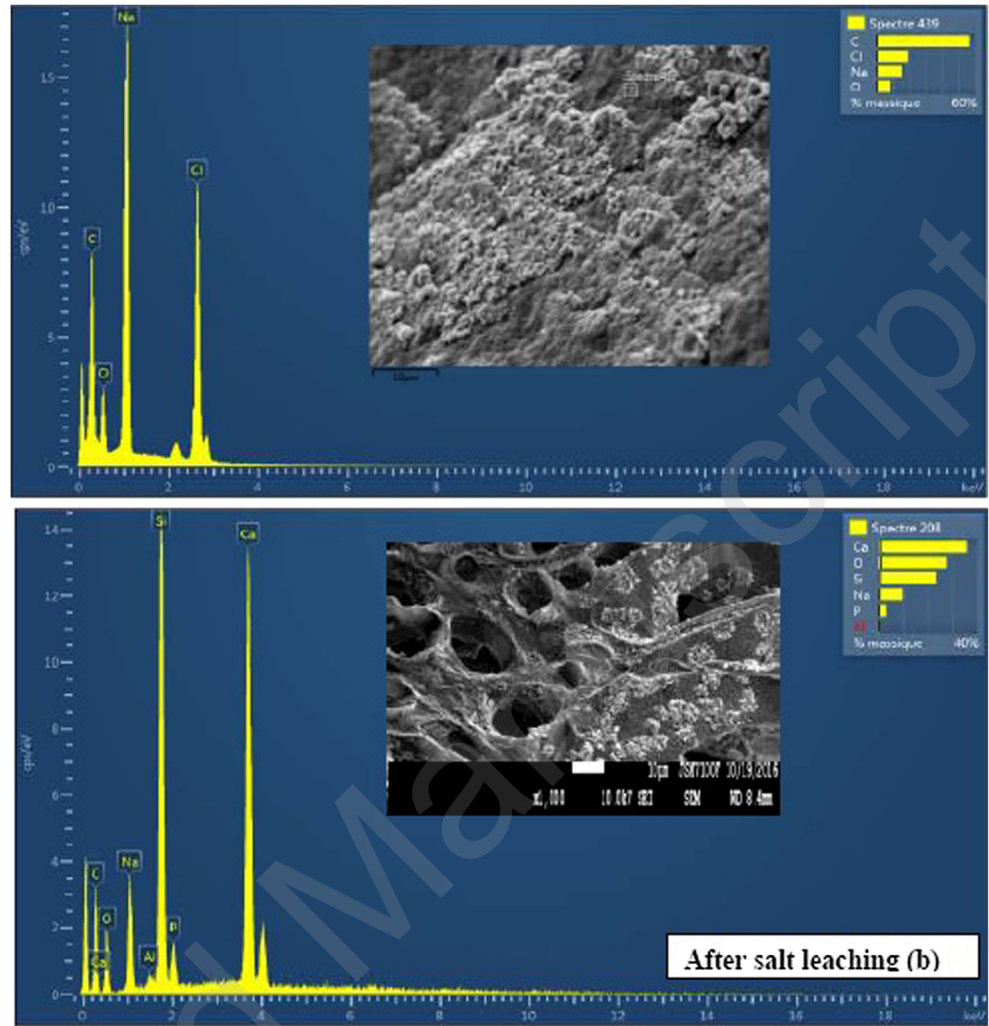


**Fig. 5** Diffractograms

Fig. 6 EDS analysis



351 **Specific surface area**

352 The specific surface area represents the total area per 1 g of  
 353 sample. It is therefore necessary to consider the entire surface  
 354 of each particle, open porosity included. The physical

principle, recognized for the determination of the specific sur- 355  
 face, is based on the adsorption of gas at low temperature. It 356  
 allows a measurement without modification of the geometri- 357  
 cal texture of the sample and determining the area of the entire 358  
 surface of the powder particles, including the surface of the 359  
 open pores accessible to the external gas molecules. 360

Figure 9 shows a progression of the specific surface area of 361  
 SLUP scaffolds by increasing the chitosan rate in there, which 362  
 varies between 20 and 37 m<sup>2</sup> g<sup>-1</sup>. This increase is much more 363  
 remarkable when applying the salt-leaching technique compared 364  
 with the loyalty method, which showed a slight increase 365  
 in a low specific surface area. 366

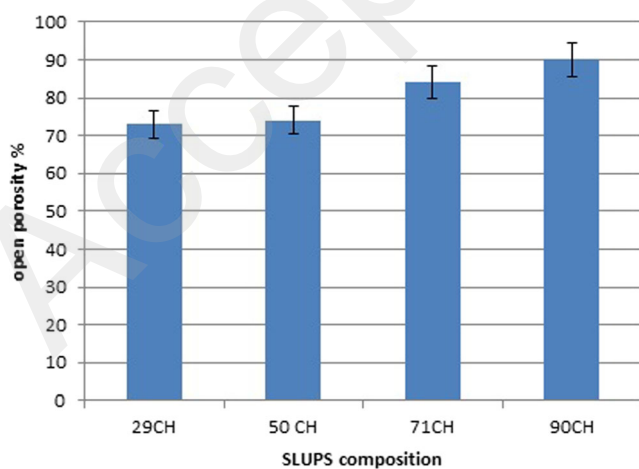
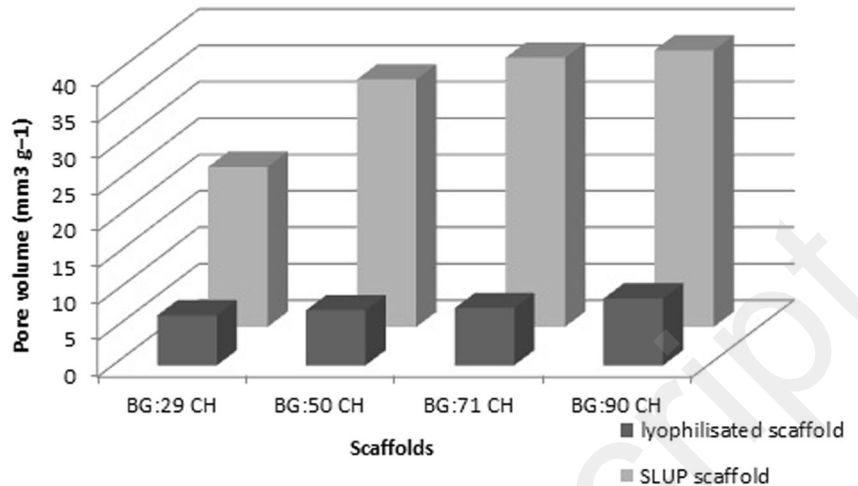


Fig. 7 SLUPS composition

Table 3 Porosity rate according to the composition of SLUP scaffolds t3.1

Sample: SLUP	Porosity %	Sample LS	Porosity %
SLUP29	73	LS29	12
SLUP50	75	LS50	16
SLUP71	95	LS71	22
SLUP90	90	LS90	31

**Fig. 8** BET measures comparing SLUPS with LS



367 This increase is much more important when applying the  
 368 SLUP technique compared with the conventional chemical  
 369 method, which showed a slight increase in a low specific  
 370 surface area.

### 371 **BET analysis nitrogen**

372 Porosity was evaluated by Brunauer–Emmet–Teller (BET)  
 373 method using Micromeritics ASAP analyzer Isotherms of  
 374 SLUP scaffolds as shown in Fig. 10.

375 All samples exhibited isotherms of type IV based on the  
 376 IUPAC classification. According to the International Union of  
 377 Pure and Applied Chemistry (IUPAC) classification, the ob-  
 378 tained isotherms (Fig. 10) belong to type H3. The curves of  
 379 adsorption and desorption form a hysteresis loop. The hystere-  
 380 sis cycle is due to the capillary condensation phenomenon  
 381 characteristic of mesoporous material (pore diameter be-  
 382 tween 2 nm and less than 50 nm). On each hysteresis cycle,  
 383 shoulders, characteristic of several families of mesoporous  
 384 materials, are observed at  $P/P_0 = 0.5$ .

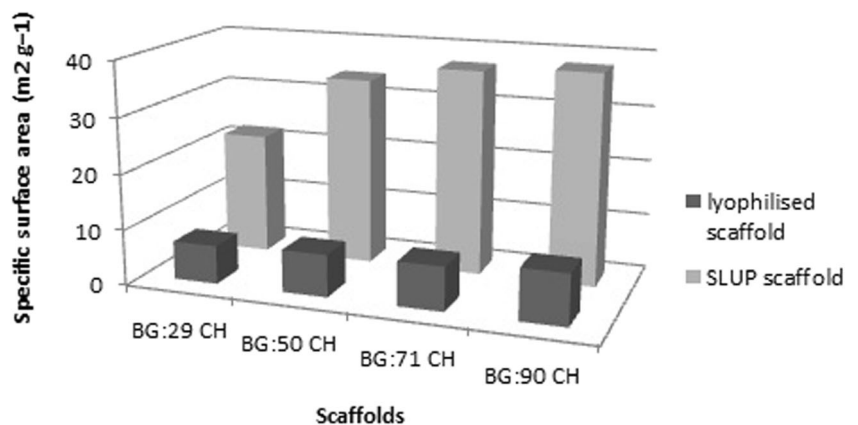
### 385 **Pores size control**

386 In this process, we used porogen as a porosity control  
 387 tool. This analysis was done to verify the hypothesis of  
 388 the dependence of the pore size as well as the homoge-  
 389 neity of porosity on the particle size of the porogen. For  
 390 this purpose, we have worked with a range of porogen  
 391 varying each time the particle size. The pores have the  
 392 same size as the porogen particles. The SEM photos of  
 393 these composites clearly show the change in pore size  
 394 from one composite to another relative to the change in  
 395 pore size. We can deduce that pores take the same size  
 396 of porogen particles as confirmed by SEM graphs  
 397 (Fig. 11).

### 398 **Influence of porogen rates on the specific surface 399 and porosity volume of scaffold SLUPS**

400 Using the proposed SLUP technique, the specific surface  
 401 and porosity volume could be easily controlled via a sim-  
 402 ple procedure, as depicted in Fig. 12. It has been noticed

**Fig. 9** Progression of the specific surface area of SLUP scaffolds by increasing the chitosan rate



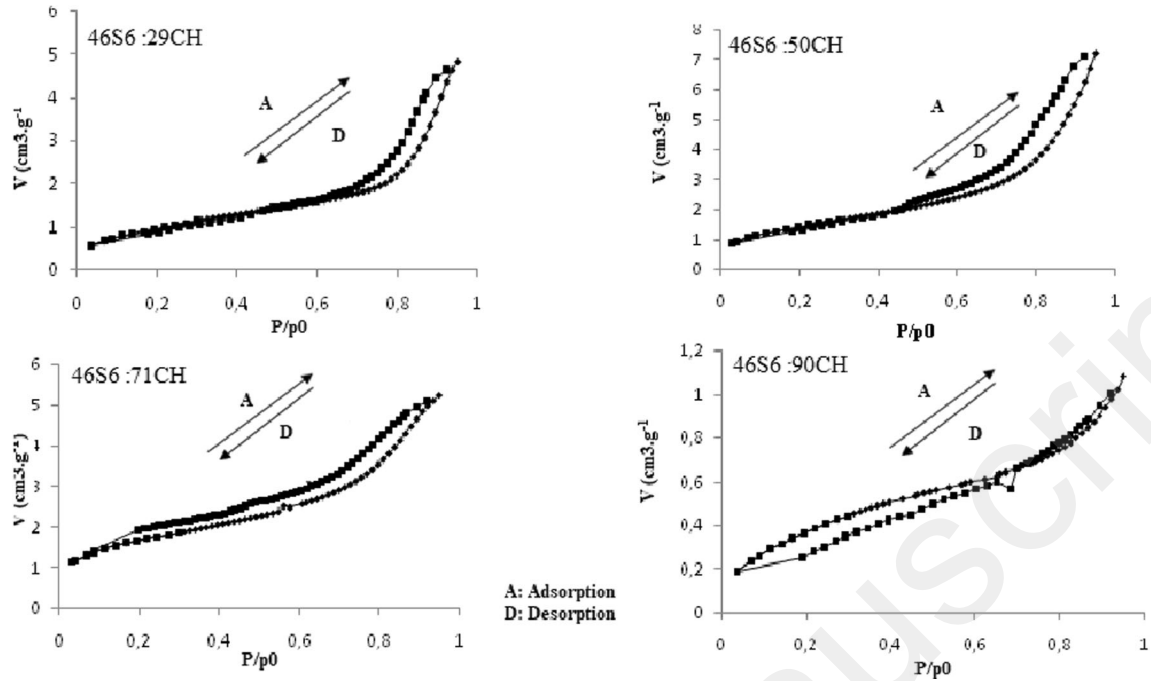


Fig. 10 Porosity evaluated by Brunauer–Emmet–Teller (BET) method using Micromeritics ASAP analyzer Isotherms of SLUP scaffolds

403 that the pore volume increases by increasing the rate of  
 404 porogen in the composition of the scaffold (Fig. 12), which  
 405 allows to control pore's volume and to have the pore vol-  
 406 ume of the requested pore.

### Kinetic of the chemical reactivity of SLUPS

407

The XRD patterns of the glass after soaking in SBF for differ-  
 408 ent periods confirm the formation of carbonated  
 409

Fig. 11 SEM graphs of parogen particles

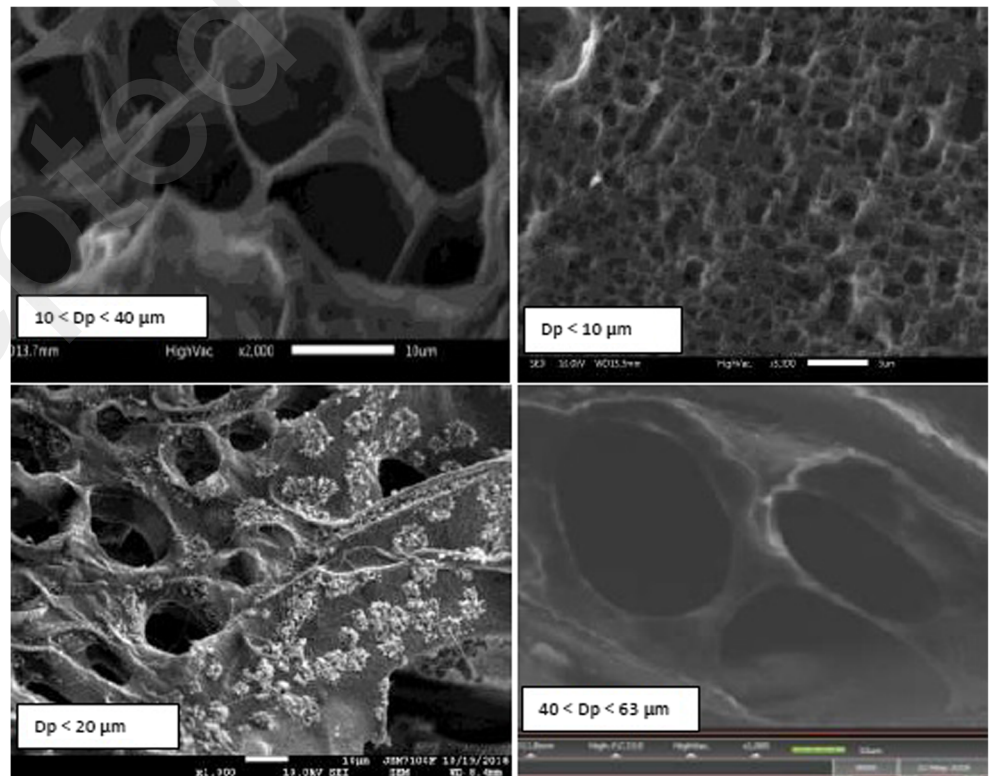
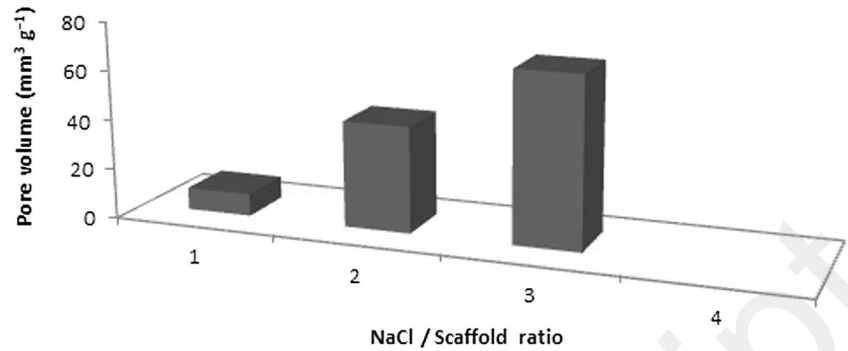


**Fig. 12** Pore volume increases by increasing the rate of porogen in the composition of the scaffold



410 hydroxyapatite (HCA) on the surface of SLUPS. Figure 13  
 411 shows the XRD patterns for SLUPS 50 before and after  
 412 soaking in SBF at different time intervals (24, 48, and 72 h).  
 413 After 24 h of soaking in SFB solution, two characteristic peaks  
 414 of hydroxyapatite at 25.80° and 31.79° were observed. The  
 415 intensity of the peaks increases with increasing time of  
 416 soaking to 3 days. These results highlight the high bioactivity  
 417 of SLUP scaffolds.

418 **Porogen effects on the kinetic of the chemical**  
 419 **reactivity**

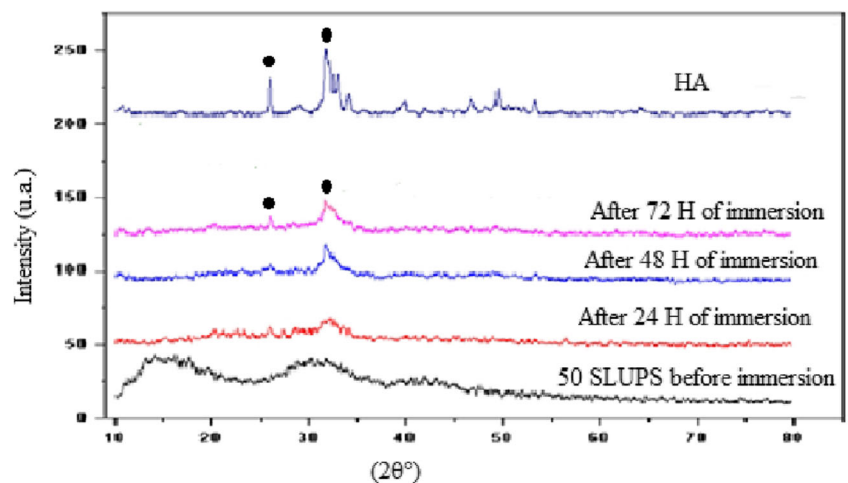
420 Evolutions of silicon, calcium, and phosphorus concentra-  
 421 tions in SBF, measured by ICP-OES, versus soaking time,  
 422 are presented in Fig. 14. The evolution of the concentrations  
 423 of all these elements followed a similar trend: strong evolu-  
 424 tion within the first 3 days. The concentration of silicon  
 425 increased during the first 24 h. At the same time, the calcium  
 426 and phosphorus concentration decreased. The evolution of  
 427 silicon concentration in SBF clearly indicated that a dissolu-  
 428 tion of the glass occurred during the first hour after soaking.  
 429 This evolution is due to the high porosity of SLUP scaffold.  
 430 The decrease of the calcium and phosphorous concentration

431 indicated that there was a calcium and phosphorus uptake by  
 432 the glass surface.

433 The effect of the presence of porogen on the reactivity of  
 434 the SLUPS surface has been studied. A total of 50 SLUPS and  
 435 50 LS were selected for testing in vitro. Evolution of silicon,  
 436 calcium, and phosphorus concentrations in SBF, measured by  
 437 ICP-OES versus soaking time, are presented on Fig. 14a-c,  
 438 respectively.

439 For SLUPS, the Si concentration increases from 0 to  
 440 52 ppm in the first 24 h, while for the LS, the Si concen-  
 441 tration increases to only 25 ppm. Therefore, the release of  
 442 the silica and, consequently, the dissolution of SLUPS occur  
 443 during 24 h. The same applies to the calcium and phos-  
 444 phorus, their concentrations in SBF decrease after 24 h in  
 445 the case of SLUPS than LS. For more information on evo-  
 446 lution of calcium and phosphorus concentration in SBF, we  
 447 have analyzed these concentrations for a short soaking  
 448 time. After 24 h, the concentration of calcium increases  
 449 from 180 to 370 ppm and of phosphorus from 75 to  
 450 65 ppm during the first 24 h. In conclusion, the presence  
 451 of porogen affects fragility and porosity, which increases  
 452 the ion exchanges and consequently the bioactivity  
 453 improvement.

**Fig. 13** XRD patterns for SLUPS 50 before and after soaking in SBF at different time intervals (24, 48, and 72 h)



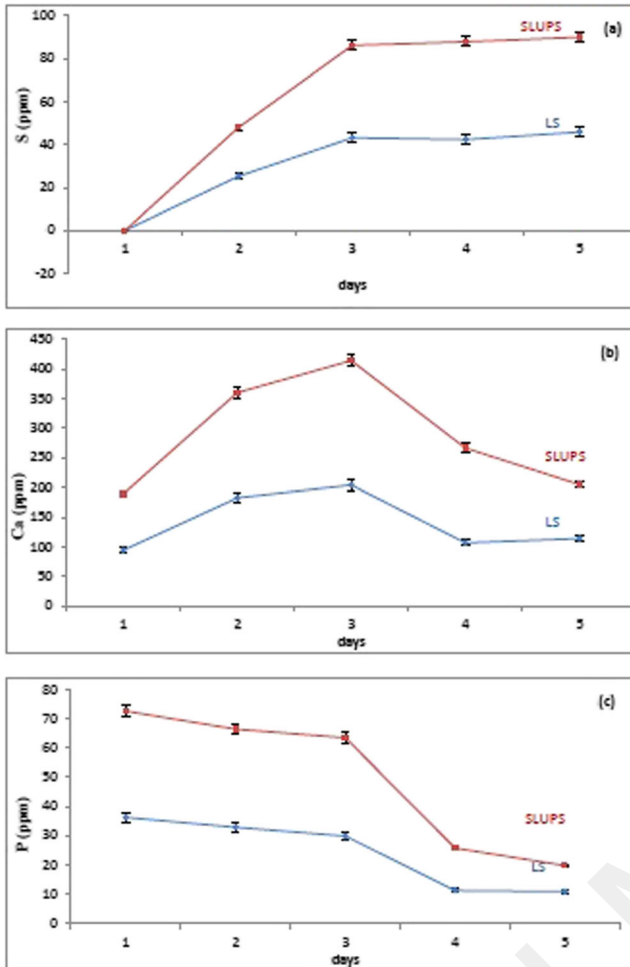


Fig. 14 Evolutions of silicon (a), calcium (b), and phosphorus (c) concentrations in SBF, measured by ICP-OES, versus soaking time

## Conclusion

454

455 In this work, we proposed a novel method known as SLUP,  
 456 which complements the disadvantages of the conventional  
 457 salt-leaching method. Thus, SLUP does not require solvent  
 458 or high pressure. Furthermore, SLUP provides scaffolds with  
 459 higher porosity than that of the conventional salt-leaching  
 460 scaffolds. The present study demonstrates a new method to  
 461 modify the surface of porous scaffolds based on the solution  
 462 casting and salt-leaching technique of chitosan-based hybrid  
 463 polymer scaffolds. The porosity of the scaffolds showed high  
 464 porosity. The SEM observations showed the increases of pore  
 465 size interconnectivity. It can be concluded that salt leaching is  
 466 a potential technique for chitosan-based scaffolds and can  
 467 contribute to improve significantly their physicochemical  
 468 properties. This simple salt-leaching process can be potential-  
 469 ly applied to various biodegradable scaffolds for tissue engi-  
 470 neering. This phenomenon can be understood as a result of the  
 471 well-interconnected structure shown in the SEM image of the  
 472 SLUP scaffold. Moreover, to reveal the simplicity and ex-  
 473 pandability of the proposed scheme, that is, SLUP, a three-

layer scaffold, with each layer having a different porosity and  
 pore size, was fabricated. Thus, the SLUP (salt leaching using  
 powder) technique may be a promising method for fabricating  
 a scaffold in lab-scale experiments because when using SLUP,  
 it is easy and facile to fabricate a well-interconnected scaffold  
 with well-defined geometry.

474  
 475  
 476  
 477  
 478  
 479

**Acknowledgments** The authors gratefully acknowledge François  
 Cheviré and Franck Tessier for the X-ray diffraction analysis, Odile  
 Merdrignac-Conanec and Nathalie Herbert for BET measurements, and  
 Francis GOUTTEFANGEAS, Loic JOANNY (CMEBA), and Christophe  
 Calers for scanning electron microscopy analysis, CMEBA.

480  
 481  
 482  
 483  
 484

## References

485Q9

1. Mezahi, F., Oudadesse, H., Harabi, A., Lucas-Girot, A., Le Gal, Y.,  
 Chair, H., Cathelineau, G.: Dissolution kinetic and structural be-  
 havior of natural hydroxyapatite vs. thermal treatment, Comparison  
 to synthetic hydroxyapatite. *J. Therm. Anal. Calorim.* **95**(21), 546–  
 555 (2008) 486
2. Letaïef, N., Lucas-Girot, A., Oudadesse, H., Dorbez-Sridi, R.,  
 Boullay, P.: Investigation of the surfactant type effect on character-  
 istics and bioactivity of new mesoporous bioactive glass in the  
 ternary system  $\text{SiO}_2 - \text{CaO} - \text{P}_2\text{O}_5$ : structural, textural and reactiv-  
 ity studies. *Microporous Mesoporous Mater.* **195**, 102–111 (2014) 487
3. Laurencin, C., Khan, Y., El-Amin, S.F.: Bone graft substitutes.  
*Expert Rev. Med. Dev.* **3**(1), 49–57 (2006) 488
4. Ducheyne, P., Qui, Q.: Bioactive ceramics: the effect of surface  
 reactivity on bone formation and bone cell function. *Biomaterials.*  
**20**(23–24), 2287–2303 (1999) 489
5. Ilan, D.I., Ladd, A.L.: Bone graft substitutes. *Oper. Tech. Plast.*  
*Reconstr. Surg.* **9**(4), 151–160 (2002) 490
6. Johnson, R.D., Todd, R.J., Arnold, F.H.: Multipoint binding in  
 metal-affinity chromatography II. Effect of pH and imidazole on  
 chromatographic retention of engineered histidine-containing cyto-  
 chromes c. *J. Chromatogr. A.* **725**(2), 225–235 (1996) 491
7. Nasrabadi, B., Mehrasa, M., Rafienia, M., Bonakdard, S., Behzad,  
 T., Gavanjia, S.: Porous starch/cellulose nanofibers composite pre-  
 pared by salt leaching technique for tissue engineering. *Carbohydr.*  
*Polym.* **108**, 232–238 (2014) 492
8. Zhuanga, P.Y., Li, Y.L., Fan, L., Lin, J., Hu, Q.L.: Modification of  
 chitosan membrane with poly(vinyl alcohol) and biocompatibility  
 evaluation. *Int. J. Biol. Macromol.* **50**(3), 658–663 (2012) 493
9. Hutmacher, D.W.: Scaffolds in tissue engineering bone and carti-  
 lage. *Biomaterials.* **21**(24), 2529–2543 (2000) 494
10. Liebschner, M.A.K., Wettergreen, M.A.: Optimization of bone  
 scaffold engineering for load bearing applications. *Topics in*  
*Tissue Engineering.* **23**, 345–362 (2003) 495
11. Rakovsky, A., Gotman, I., Rabkin, E., Gutmanas, E.Y.: Strong bio-  
 resorbable Ca phosphate-PLA nanocomposites with uniform phase  
 distribution by attrition milling and high pressure consolidation. *J.*  
*Mech. Behav. Biomed. Mater.* **18**, 37–46 (2013) 496
12. Kim, T.G., Chung, H.J., Park, T.G.: Macroporous and nanofibrous  
 hyaluronic acid/collagen hybrid scaffold fabricated by concurrent  
 electrospinning and de- position/leaching of salt particles. *Acta*  
*Biomater.* **6**(4), 1611–1619 (2008) 497
13. Hollander, A.P., Hatton, P.V.: Biopolymer Methods in Tissue  
 Engineering. *Methods Mol. Biol.* **238**, (2004) 498
14. Cho, Y.S., Hong, N.M., Kim, S.Y., Lee, S.J., Lee, J.H., Kim, Y.,  
 Cho, Y.S.: Fabrication of dual-pore scaffolds using SLUP (salt  
 leaching using powder) and WNM (wire-network molding) tech-  
 niques. *Mater. Sci. Eng.* **45**, 546–555 (2014) 499

500  
 501  
 502Q10  
 503  
 504  
 505  
 506  
 507  
 508  
 509  
 510  
 511  
 512  
 513  
 514  
 515  
 516  
 517  
 518Q11  
 519  
 520  
 521  
 522  
 523  
 524  
 525  
 526  
 527  
 528  
 529  
 530  
 531  
 532

533	15.	Park, H.J., Lee, O.J., Lee, M.C., Moon, B.M., Ju, H.W., Jm, L., Kim, J.H., Kim, D.W., Park, C.H.: Fabrication of 3D porous silk scaffolds by particulate (salt/sucrose)leaching for bone tissue reconstruction. <i>Int. J. Biol. Macromol.</i> <b>78</b> , 215–223 (2015)	571
534			572
535			573
536			574
537	16.	Cannillo, V., Chiellini, F., Fabbri, P., Sola, A.: Production of Bioglass® 45S5–polycaprolactone composite scaffolds via salt-leaching. <i>Compos. Struct.</i> <b>92</b> (8), 1823–1832 (2010)	575
538			576
539			577
540	17.	Ezequiel, C.-J.S., Edel Barbosa-Stancioli, F., AlexandraMansur, A.P., Wander Vasconcelos, L., HermanMansur, H.: Preparation and characterization of chitosan/poly(vinyl alcohol) chemically crosslinked blends for biomedical applications. <i>Carbohydr. Polym.</i> <b>76</b> (3), 472–481 (2009)	578
541			579
542			580
543			581
544			582
545	18.	Kamoun, E.A., Kenawy, E.S., Tamer, M.T., El-Meligy, A.M., MohyEldin, S.M.: Poly (vinyl alcohol)-alginate physically crosslinked hydrogel membranes for wound dressing applications: characterization and bio-evaluation. <i>Arab. J. Chem.</i> <b>8</b> (1), 38–47 (2015)	583
546			584
547			585
548			586
549			587
550	19.	Yu, S.H., Tsai, M.L., Lin, B.X., Lin, C.W., Mi, F.L.: Tea catechins-cross-linked methyl- cellulose active films for inhibition of light irradiation and lipid peroxidation induced $\beta$ -carotene degradation. <i>Food Hydrocoll.</i> <b>44</b> , 491–505 (2015)	588
551			589
552			590
553			591
554	20.	Kanimozhi, K., Khaleel Basha, S., Sugantha Kumari, V.: Processing and characterization of chitosan/PVA and methylcellulose porous scaffolds for tissue engineering. <i>Mater. Sci. Eng.</i> <b>61</b> (1), 484–491 (2016)	592
555			593
556			594
557			595
558	21.	Trong, M., Chia-Fong, K., Wen-Yen, C., Ching, A.: Preparation and characterization of chitosan-g-poly (vinyl alcohol)/poly(vinyl alcohol) blends used for the evaluation of blood-contacting compatibility. <i>Carbohydr. Polym.</i> <b>63</b> (3), 331–339 (2006)	596
559			597
560			598
561			599
562	22.	Collins, M.N., Colin, B.: Hyaluronic acid based scaffolds for tissue engineering. <i>Carbohydr. Polym.</i> <b>92</b> (2), 1262–1279 (2013)	600
563			601
564	23.	Seitz, H., Rieder, W., Irsen, S., Leukers, B., Tille, C.: Three-dimensional printing of porous ceramic scaffolds for bone tissue engineering. <i>Biomed. Mater. Res.</i> <b>74</b> (2), 782–788 (2005)	602
565			603
566			604
567	24.	Wers, E., Oudadesse, H., Lefevre, B., Merdrignac-Conanec, O., Barroug, A.: Evaluation of the kinetic and relaxation time of gentamicin sulfate released from hybrid biomaterial Bioglass-chitosan scaffolds. <i>Appl. Surf. Sci.</i> <b>353</b> , 200–208 (2015)	605
568			606
569			
570			
607			